Improved Dynamics in DC-DC Converters for IoT Applications with Repetitive Load Profiles Using Self-Calibrated Preemptive Current Control

D.K.W. Li[1], Z. Gong[1], M. Rose[2], H.J. Bergveld[2], and O. Trescases[1]
[1]University of Toronto, Toronto, ON, Canada
[2]NXP Semiconductors, Eindhoven, The Netherlands
Email: davidking.li@mail.utoronto.ca

***Abstract*—This paper presents a novel approach to improve the dynamic response of inductive dc-dc converters in applications having repetitive load profiles. In many Internet-of-Things (IoT) applications, such as wireless sensor networks (WSN), the load current profile has a periodic nature, and is therefore predictable by the power management circuits. This unique nature is exploited by the proposed Preemptive Concurrent Controller (PCC) to achieve a dynamic response superior to the theoretical limits of time-optimal control. The preemptive controller ramps up the inductor current prior to the occurrence of a load step and reduces the required output capacitance. The non-inverting buck-boost converter is used in this work and operates with a freewheeling mode that avoids output voltage overshoot during the preemptive inductor current ramp. Two hysteric control loops operate concurrently to define the freewheeling interval. A simple digital calibration scheme is demonstrated to extract timing and amplitude features from a load current profile in order to optimize the timing of the preemptive current reference in the next cycle. Freewheeling is thus minimized to increase system efficiency. The PCC and associated load profile learning algorithm is experimentally verified and uses $10\times$ less capacitance compared to the time-optimal control benchmark.**

I. Introduction

In 2015, the U.S. Government spent $8.8 billion on Internet-of-Things (IoT) devices [1]. The future widespread deployment of IoT devices in wireless sensor networks (WSN) has a strong disruptive potential in sectors ranging from agriculture, energy, consumer, to transportation and security. Modern IoT designs must compromise between size, weight, cost, and battery life to be commercially viable [2]. Despite advances in Power-Supply-on-Chip (PwrSOC) technology [3]–[5], inductance and capacitance on the order of μH/μF remain impractical to integrate cost-effectively in silicon. As a result, discrete components that consume a significant portion of the device volume remain a requirement for dc-dc power solutions for IoT.

The architecture of a typical IoT device is shown in Fig. 1. In addition to the energy harvester and upstream converter responsible for charging the energy storage from the energy harvester, most devices also include a battery source to supply the loads through one or more dc-dc converters. IoT devices are designed to operate in a periodic and predictable manner due to the desire for autonomous deployment in remote areas [6]–[10]. As shown in Fig. 2, regardless of the specific application, an IoT device deployed in a WSN typically spends over 90% of its deployment time in sleep mode and only periodically wakes up to perform an operational cycle. The IoT cycle with period T_c consists of measurement, processing and wireless transmission steps. The current profile during the full cycle is typically weakly data-dependent. From the perspective of the downstream battery-to-load power converters, this translates into a periodic and predictable load current profile.

The focus of this work is to improve the dynamic response of the downstream converter by leveraging the periodic behaviour of IoT systems. The hypothesis is: *with a predictable load, a power converter can preemptively adjust its inductor current to match the dynamic demands of the load, thus reducing the output capacitance requirement.*

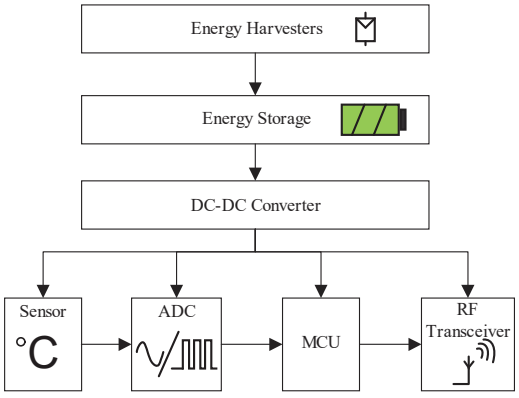

Fig. 1. Simplified IoT-WSN hardware architecture.

Time-optimal control (TOC), as shown in Fig. 3, has been widely used to reduce output capacitance of buck converters in the presence of load steps [11]–[15]. The minimum response time, t_{res}, in Fig. 3 is given by

$$t_{res} = \frac{\Delta I_{out} L}{V_{in} - V_{out}} \left(1 + \sqrt{1 + \frac{V_{in} - V_{out}}{V_{out}}}\right), \qquad (1)$$

which is only valid for large load current steps, ΔI_{out}, relative to the steady-state inductor current ripple, ΔI_L. From

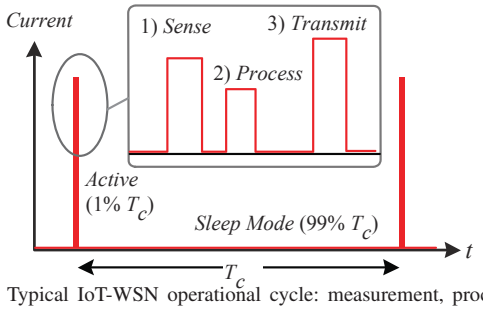

Fig. 2. Typical IoT-WSN operational cycle: measurement, processing and wireless transmission steps.

(1), t_{res} is directly proportional to ΔI_{out} and L, which shows the physical limitation imposed by the inductive energy transfer, irrespective of the controller architecture or the switching frequency. Assuming negligible effective series resistance, the best-case output droop voltage ΔV_{res} is given by:

$$\Delta V_{res} = \frac{Q_1}{C_{out}} = \frac{\Delta I_{out}^2}{2C_{out}m_1} = \frac{\Delta I_{out}^2 L}{2C_{out}(V_{in} - V_{out})}. \quad (2)$$

Using this non-linear control scheme, the required capacitance is considered to be an absolute minimum for a given voltage deviation ΔV_{res}. A Preemptive Concurrent Control (PCC) scheme is demonstrated in this work to exploit the periodic nature of the load current in IoT applications. The PCC scheme improves the dynamic response of dc-dc converters beyond the theoretical limits of time-optimal control predicted from (1) and (2).

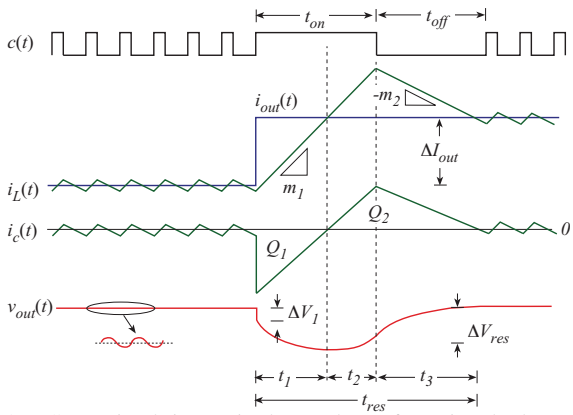

Fig. 3. Conventional time-optimal control waveforms in a buck converter. With this non-linear control, the response time is primarily limited by the inductance value.

II. Theoretical Operation of Preemptive Concurrent Control

In this work, the load voltage V_{out} = 3.3 V overlaps with the single-cell lithium battery range V_{in} = 2.7-4.3 V, and a non-inverting buck-boost (NIBB) topology [16] is used to accommodate the buck-boost requirement. The NIBB is shown in Fig. 4 and is operated in either buck or boost mode depending on V_{in}. The scope in this paper is limited to buck mode. In addition to these conventional operating modes, a freewheeling segment can be introduced to the switching sequence in which the inductor is short-circuited and no energy is drawn from the source or delivered to the load [17]. This additional mode of operation is a key requirement for preemptive control.

A. Preemptive Concurrent Control

Concurrent control refers to the simultaneous and independent operation of two hysteretic control loops, a current loop using the input-side half-bridge, $M1$ and $M2$, and a voltage loop using the output-side half-bridge, $M3$ and $M4$. This is in contrast to a traditional nested architecture, where the outer voltage loop provides a reference for the inner current loop [18], [19]. In this case the current reference I_{cmd} comes from the output of the preemptive supervisory module and represents a calibrated load forecast. In the four-switch NIBB topology, the freewheeling mode occurs when $M2$ and $M4$ are *on*, and its availability allows the voltage loop to regulate V_{out} even if the inductor current I_L is greater than the load current I_{load}. The freewheeling segment therefore allows $i_L(t)$ to be ramped up *prior* to the load step without causing an overvoltage event on V_{out}, making a reduction in C_{out} possible at the expense of slightly higher conduction and switching loss.

The operation of PCC prior to calibration is shown in Fig.5(a), where I_{cmd} is constantly higher than I_{load} and regular freewheeling is required to maintain voltage regulation as load steps occur. The ideal post-calibration waveform is shown in Fig.5(b), where $i_L(t)$ is preemptively regulated to reach I_{load} prior to the positive load step and after the negative load step. In this case, the total freewheeling time is minimized and thus the efficiency is maximized. As with all hysteretic control schemes, the PCC switching frequency is variable. Solutions involving phase-locked loops [20] can be applied to regulate frequency. Freewheeling can also be introduced to other NIBB control schemes such as pulse-width modulation through a nonlinear ramping interval, or to other converter topologies such as buck or boost through an additional freewheeling switch [17]. These options are beyond the scope of this work.

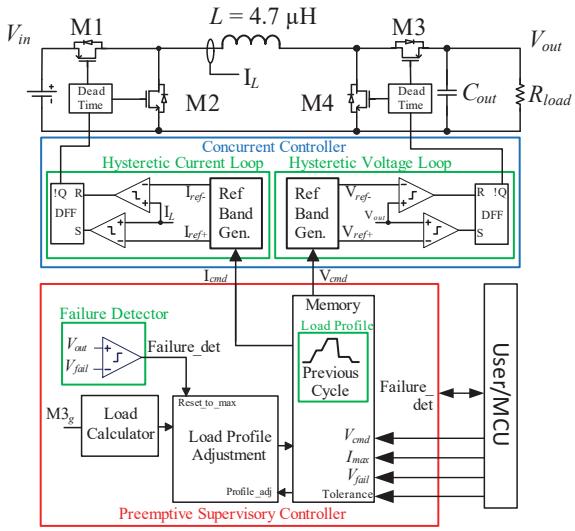

Fig. 4. Architecture of Preemptive Concurrent Control.

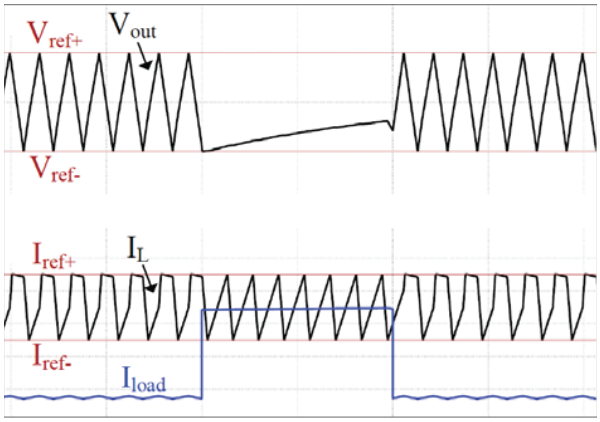

(a)

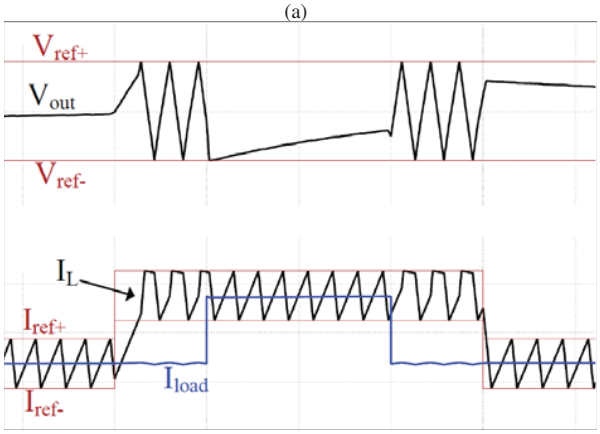

(b)

Fig. 5. PCC operation in buck mode (a) prior to calibration, with excessive freewheeling and (b) post-calibration, with adjusted reference current timing such that freewheeling is minimized and efficiency maximized. I_{ref+}, I_{ref-}, V_{ref+}, and V_{ref-} refer to the hysteretic control band limits around I_{cmd} and V_{cmd}.

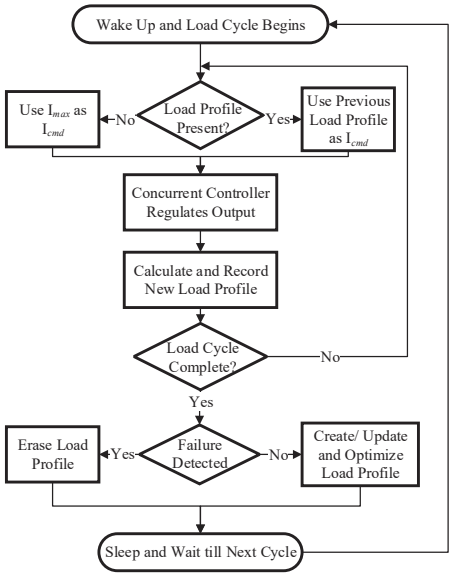

Fig. 6. Preemptive control scheme, including the load forecast calibration process.

B. Calibration of Preemptive Control: Load Feature Extraction

In order to fully leverage the dynamic advantages of preemptive control while minimizing the efficiency penalty, the PCC is designed to optimize both the timing and amplitude of I_{cmd} according to the repetitive load profile. This is achieved through load profiling and feature extraction, as outlined in Fig. 6. By examining the M3 on-time $t_{M3,on}$ and the average inductor current approximated as I_{cmd} over the M3 switching period $t_{M3,period}$, the average load current I_{load} during the period can be approximated by:

$$I_{load} = I_{cmd}\frac{t_{M3,on}}{t_{M3,period}}. \quad (3)$$

Using the approximated load profile obtained from (3), the preemptive controller calibrates its predictions every load-step cycle. Since the exact load profile is not precisely known at startup, which is true even in cases where the power management and load circuits are integrated together, this technique requires the system to meet several conditions:

1) The maximum possible load current must be known
2) The load profile must be repetitive (within a defined tolerance to account for data dependency and timing jitter)
3) The system must be tolerant of single-cycle communication failure at startup due to the risk of under-voltage

Nevertheless, as previously mentioned, these three conditions can be met for most IoT-WSN applications.

III. Experimental Results

The system shown in Fig. 4 was implemented on hardware as in Fig. 7. The experimental setup was realized with a 4.7 μH inductor and an output capacitance of 21.4 μF when operating with TOC and 2 μF when operating with PCC. The input voltage was 4.5 V and the output average voltage was 3.3 V. The passive components and voltage operating point were selected to achieve a target switching frequency of 1 MHz while meeting the voltage specification of a Zigbee wireless transceiver, which has a nominal V_{DD} of 3.3 V and an operational range of 3-3.6 V. For the purpose of demonstration, a Xilinx Spartan-3E FPGA was used to implement the control and calibration algorithms of the PCC, but the goal is an on-chip implementation of the complete power management scheme.

For this experiment, the TOC was used as a baseline comparison for the PCC. Outside of the load step, the TOC reverts to hysteretic current-mode control with a PI compensator in the voltage loop. Two load resistors controlled by the microprocessor through MOSFET switches (not shown) are used to simulate the wireless transceiver load steps. This transceiver load emulation provides maximum flexibility for designing the PCC.

The baseline response of TOC to positive and negative load steps is shown in Figs. 8(a) and (b), respectively. The PCC response under the same conditions is shown in Figs. 9(a) and (b). The PCC has a $10\times$ smaller capacitor (2 μF versus 21.4

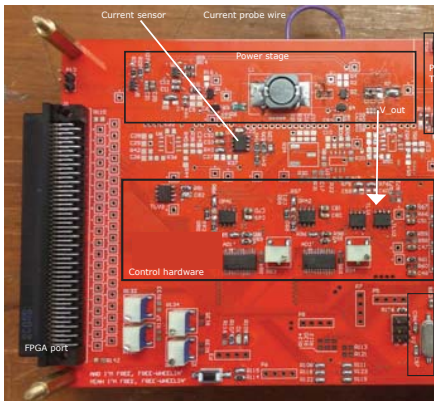

Fig. 7. Experimental setup of the PCC

μF for TOC) and maintains continuous voltage regulation at about 60 mV ripple amplitude due to the hysteretic control band, while the maximum voltage deviation under the TOC is 90 mV with a transient duration of about 6 μs. The advantage of the PCC over TOC for capacitance reduction is apparent upon comparison of the transient responses shown in Figs. 8 and 9.

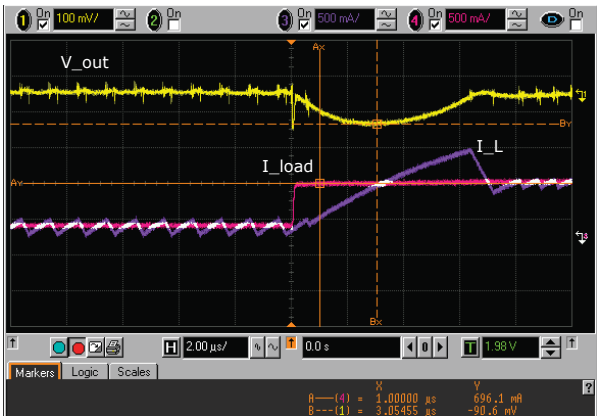

(a)

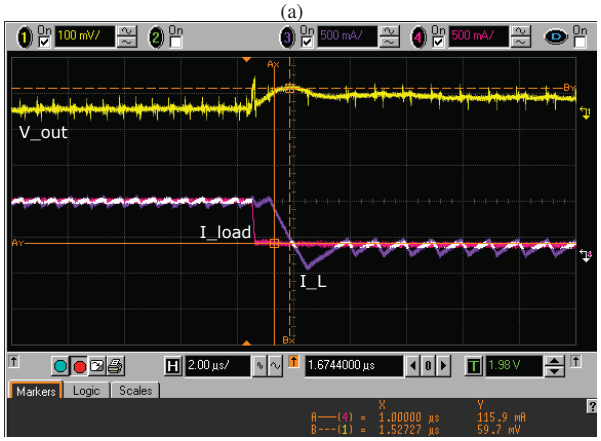

(b)

Fig. 8. Dynamic response to (a) a positive load step, and (b) a negative load step using time optimal control. Cursor A shows the step current and cursor B shows the voltage spike or droop.

The operation of the load profile learning algorithm is

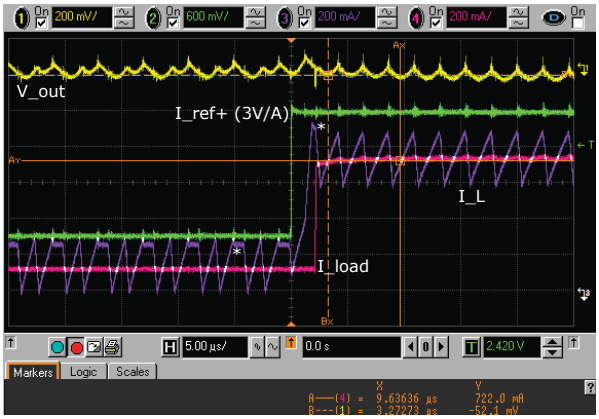

(a)

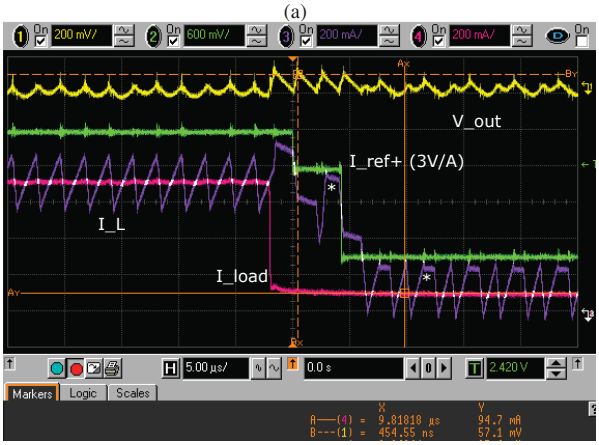

(b)

Fig. 9. Dynamic response to (a) a postive load step and (b) a negative load step using preemptive concurrent control. Cursor A shows the step current and cursor B shows the voltage spike or droop, asterisks indicate examples of freewheeling events.

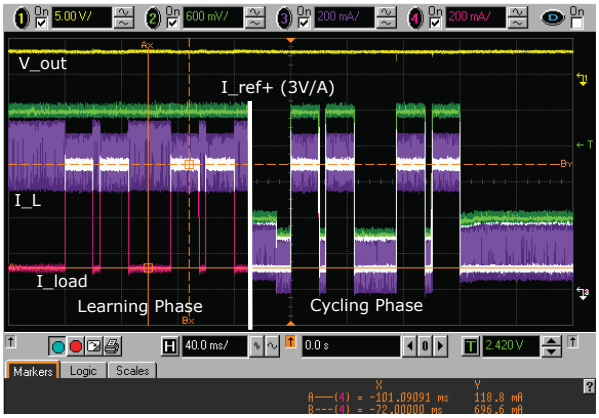

Fig. 10. Learning algorithm in operation: actual load step timings and magnitudes were taken from characterization of the XBee Pro S5 load profile.

shown in Fig. 10. The increase in time during which I_{load} matches I_L on the second load cycle demonstrates the reduction in freewheeling time.

A discharge test was conducted over repeating load cycles to accurately compare the PCC's average power consumption after calibration versus the baseline TOC. The time to dis-

charge an ultracapacitor bank of 175 F from 4.6 V to 4.5 V was measured for three runs. Fig. 11 shows one example run of the discharge test. On average, the PCC was found to consume 2.7% less energy than the TOC. Since both PCC and TOC operate with variable frequency, a detailed loss analysis is required to account for slight differences, however it is promising that the use of freewheeling in the calibrated PCC has a minor efficiency impact.

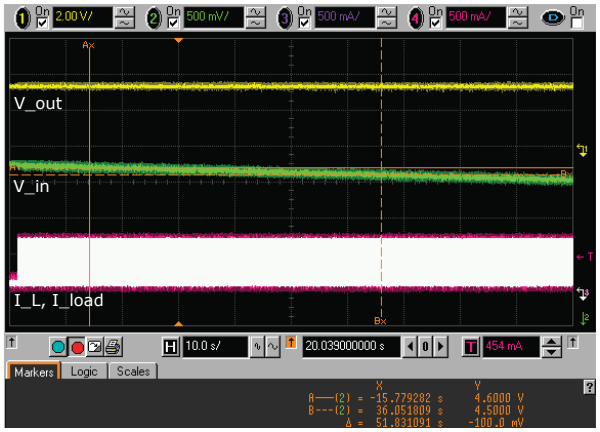

Fig. 11. Example discharge test run performed as a preliminary energy analysis.

IV. Conclusions and Future Work

The experimental results demonstrate that the PCC implemented with dual concurrent hysteric loops can achieve $10\times$ reduction in capacitor size over time-optimal control. In applications where the variable frequency operation of the PCC is undesirable, a fixed-frequency mode can be introduced following the load steps, once the system is calibrated. Future work is needed to investigate the efficiency impact of the freewheeling mode.

References

[1] A. Meola, "The us government is pouring money into the internet of things," Business Insider, May 2016.

[2] T. Lee, "The hardware enablers for the internet of things - part i," IEEE Internet of Things, Jan 2015.

[3] L. Li, D. W. Lee, K. P. Hwang, Y. Min, T. Hizume, M. Tanaka, M. Mao, T. Schneider, R. Bubber, and S. X. Wang, "Small-resistance and high-quality-factor magnetic integrated inductors on pcb," *IEEE Transactions on Advanced Packaging*, vol. 32, no. 4, pp. 780–787, Nov 2009.

[4] M. Ludwig, M. Duffy, T. O'Donnell, P. McCloskey, and S. C. O. Mathuna, "Pcb integrated inductors for low power dc/dc converter," *IEEE Transactions on Power Electronics*, vol. 18, no. 4, pp. 937–945, July 2003.

[5] Y. L. Li, T. G. Yew, C. Y. Chung, and D. G. Fugueroa, "Design and performance evaluation of microprocessor packaging capacitors using integrated capacitor-via-plane model," *IEEE Transactions on Advanced Packaging*, vol. 23, no. 3, pp. 361–367, Aug 2000.

[6] G. Stamatakis, E. Z. Tragos, and A. Traganitis, "Periodic collection of spectrum occupancy data by energy constrained cognitive iot devices," in *2015 International Wireless Communications and Mobile Computing Conference (IWCMC)*, Aug 2015, pp. 880–885.

[7] Q. M. Ashraf, M. I. M. Yusoff, A. A. Azman, N. M. Nor, N. A. A. Fuzi, M. S. Saharedan, and N. A. Omar, "Energy monitoring prototype for internet of things: Preliminary results," in *Internet of Things (WF-IoT), 2015 IEEE 2nd World Forum on*, Dec 2015, pp. 1–5.

[8] M. Healy, T. Newe, and E. Lewis, "Wireless sensor node hardware: A review," in *Sensors, 2008 IEEE*, Oct 2008, pp. 621–624.

[9] V. Raghunathan, C. Schurgers, S. Park, and M. B. Srivastava, "Energy-aware wireless microsensor networks," *IEEE Signal Processing Magazine*, vol. 19, no. 2, pp. 40–50, Mar 2002.

[10] C. C. Enz, A. El-Hoiydi, J. D. Decotignie, and V. Peiris, "Wisenet: an ultralow-power wireless sensor network solution," *Computer*, vol. 37, no. 8, pp. 62–70, Aug 2004.

[11] G. Feng, E. Meyer, and Y. F. Liu, "High performance digital control algorithms for dc-dc converters based on the principle of capacitor charge balance," in *Power Electronics Specialists Conference, 2006. PESC '06. 37th IEEE*, June 2006, pp. 1–7.

[12] P. Cheng, M. Vasic, O. Garca, J. A. Oliver, P. Alou, and J. A. Cobos, "Minimum time control for multiphase buck converter: Analysis and application," *IEEE Transactions on Power Electronics*, vol. 29, no. 2, pp. 958–967, Feb 2014.

[13] G. E. Pitel and P. T. Krein, "Minimum-time transient recovery for dc-dc converters using raster control surfaces," *IEEE Transactions on Power Electronics*, vol. 24, no. 12, pp. 2692–2703, Dec 2009.

[14] A. Radic, Z. Lukic, A. Prodic, and R. H. de Nie, "Minimum-deviation digital controller ic for dc-dc switch-mode power supplies," *IEEE Transactions on Power Electronics*, vol. 28, no. 9, pp. 4281–4298, Sept 2013.

[15] S. V. Dhople, K. A. Kim, and A. D. Domnguez-Garca, "Time-optimal control in dc-dc converters: A maximum principle perspective," in *2014 IEEE Applied Power Electronics Conference and Exposition - APEC 2014*, March 2014, pp. 2804–2808.

[16] B. Sahu and G. A. Rincon-Mora, "A low voltage, dynamic, noninverting, synchronous buck-boost converter for portable applications," *IEEE Transactions on Power Electronics*, vol. 19, no. 2, pp. 443–452, March 2004.

[17] D. Ma, W.-H. Ki, and C.-Y. Tsui, "A pseudo-ccm/dcm simo switching converter with freewheel switching," in *Solid-State Circuits Conference, 2002. Digest of Technical Papers. ISSCC. 2002 IEEE International*, vol. 2, Feb 2002, pp. 316–525.

[18] R. Redl and N. O. Sokal, "Near-optimum dynamic regulation of dc-dc converters using feed-forward of output current and input voltage with current-mode control," *IEEE Transactions on Power Electronics*, vol. PE-1, no. 3, pp. 181–192, July 1986.

[19] B. Bryant and M. K. Kazimierczuk, "Voltage loop of boost pwm dc-dc converters with peak current-mode control," *IEEE Transactions on Circuits and Systems I: Regular Papers*, vol. 53, no. 1, pp. 99–105, Jan 2006.

[20] M. S. Zaman, Y. Wen, R. Fernandes, B. Buter, T. Doorn, M. Dijkstra, H. J. Bergveld, and O. Trescases, "A cell-level differential power processing ic for concentrating-pv systems with bidirectional hysteretic current-mode control and closed-loop frequency regulation," *IEEE Transactions on Power Electronics*, vol. 30, no. 12, pp. 7230–7244, Dec 2015.